Monthly Notices
of the
ROYAL ASTRONOMICAL SOCIETY

Mon. Not. R. Astron. Soc. **405,** 657–665 (2010) doi:10.1111/j.1365-2966.2010.16490.x

Detecting circumbinary planets using eclipse timing of binary stars – numerical simulations

P. Sybilski,[1⋆] M. Konacki[1,2] and S. Kozłowski[2]

[1]*Nicolaus Copernicus Astronomical Center, Polish Academy of Sciences, Rabiańska 8, 87-100 Toruń, Poland*
[2]*Astronomical Observatory, Adam Mickiewicz University, Słoneczna 36, 60-186 Poznań, Poland*

Accepted 2010 February 4. Received 2010 February 1; in original form 2010 January 4

ABSTRACT

The presence of a body in an orbit around a close eclipsing binary star manifests itself through the light time effect influencing the observed times of eclipses as both the close binary and the circumbinary companions move around the common centre of mass. This fact combined with the periodicity with which the eclipses occur can be used to detect the companions. Given a sufficient precision of the times of eclipses, the eclipse timing can be employed to detect substellar or even planetary mass companions.

The main goal of this paper is to investigate the potential of the photometry-based eclipse timing of binary stars as a method of detecting circumbinary planets. In the models we assume that the companion orbits a binary star in a circular Keplerian orbit. We analyse both the space- and ground-based photometry cases. In particular, we study the usefulness of the ongoing *CoRoT* and *Kepler* missions in detecting circumbinary planets. We also explore the relations binding the planet discovery space with the physical parameters of the binaries and the geometrical parameters of their light curves. We carry out detailed numerical simulations of the eclipse timing by employing a relatively realistic model of the light curves of eclipsing binary stars. We study the influence of the white and red photometric noises on the timing precision. We determine the sensitivity of the eclipse timing technique to circumbinary planets for the ground- and space-based photometric observations. We provide suggestions for the best targets, observing strategies and instruments for the eclipse timing method. Finally, we compare the eclipse timing as a planet detection method with the radial velocities and astrometry.

Key words: methods: analytical – methods: numerical – techniques: photometric – binaries: eclipsing – planetary systems.

1 INTRODUCTION

Accurate light curves of eclipsing binary stars can be used to precisely measure the times of eclipses. Such eclipse timing (ET) measurements can then be compared with the predicted ones and used to infer information on, e.g., the presence of an additional body orbiting the eclipsing binary. The presence of an additional body will cause the motion of the eclipsing binary with respect to the centre of mass of the entire system and result in advances/delays in the times of eclipses due to the light time effect. This old idea (it dates back to the 17th century and Ole Roemer) has been used to, e.g., detect stellar companions to eclipsing binaries. It can also be used to detect circumbinary planets (P-type planets; Dvorak 1984). Clearly, this idea is simple and has already been explored in the literature as a potential way of detecting extrasolar planets (see e.g. Doyle & Deeg 2004; Muterspaugh et al. 2007; Deeg et al. 2008).

In this paper, we carry out detailed numerical simulations of ET to explore in more depth what can be achieved with this technique from both the ground and space. In the first part, we study the *CoRoT* and *Kepler* and investigate how their very high photometric precision (Koch et al. 2004; Alonso et al. 2008) can be used to detect circumbinary planets via ET. In the second part, we estimate the influence of the red noise and the gaps in the light curves typical for the ground-based photometry caused by, e.g., the day–night cycle, technical problems and weather conditions on the discovery space.

In Section 2, we describe the light curve and noise models used in the simulations; in Section 3, we describe how a planetary timing signal is generated and detected in a simulated light curve; in Section 4, we analyse the space missions *CoRoT* and *Kepler*; in Section 5, we discuss a ground-based effort; and in Section 6, conclusions are provided.

⋆E-mail: sybilski@ncac.torun.pl

2 LIGHT CURVE OF AN ECLIPSING BINARY AND ITS NOISE

A model of an eclipsing binary is adopted from Nelson & Davis (1972). It describes systems that do not fill their Roche lobes. We decided to examine detached binaries as such systems are the most likely ones to serve as stable clocks. The adopted model is simple enough to provide fast computations and at the same time enables an adequate description of an eclipsing binary. Eclipses are described as an obscuration of two discs. The algorithm used to compute a synthetic light curve comes from Nelson & Davis (1972) and is based on a few simple equations. Let us note that two of the equations are misprinted in Nelson & Davis (1972). The correct version for the eclipsed surface is

$$B = r_1^2 \arccos\frac{r_1 - a}{r_1} - (r_1 - a)\left(2r_1 a - a^2\right)^{1/2} + r_2^2 \arccos\frac{r_2 - b}{r_2} - (r_2 - b)\left(2r_2 b - b^2\right)^{1/2} \quad (1)$$

for the situation shown in Fig. 1 when the projected stars' separation is larger than the radius of the bigger star and

$$B = \pi r_1^2 - r_1^2 \arccos\frac{r_1 - a}{r_1} + (r_1 - a)\left(2r_1 a - a^2\right)^{1/2} + r_2^2 \arccos\frac{r_2 - b1}{r_2} - \left(2r_2 b - b^2\right)^{1/2} \quad (2)$$

for the situation shown in Fig. 2. In the above B is the obscured surface, r_1 and r_2 denote the radii of the first and second stars, respectively, a, b are shown in Fig. 2 and $\cos\alpha = \frac{r_2 - b}{r_2}$, $\cos\Psi = \frac{r_1 - a}{r_1}$. The remaining symbols are as in the original article.

In the above description, the local perspective effect is ignored. In a typical realistic case, the separation between the stars is very small compared to the distance between the observer and binary. The parameters describing the system are the separation a, radii of the first and second stars r_1 and r_2, respectively, the total luminosity L, the fraction of light emitted by the second component L_2 and the Keplerian elements of the planetary and binary orbits (ellipticity, inclination, semimajor axis). Both orbits, of the planet and of the binary star, are Keplerian. We assume that the perturbing planet changes only the position of the binary stars' centre of mass and not of the orbital elements. In our simulations, we assume circular orbits.

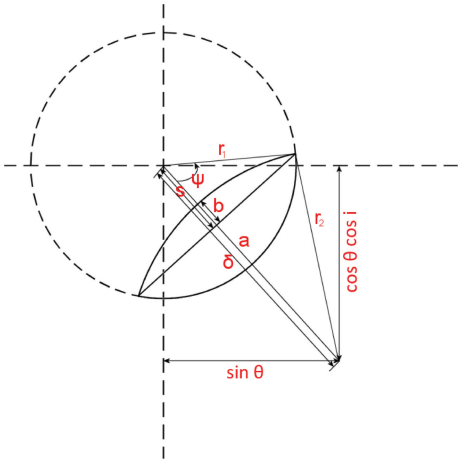

Figure 1. The first type of an occultation when the projected stars' separation is larger than the radius of the bigger star. The symbols are described in the text and in Nelson & Davis (1972).

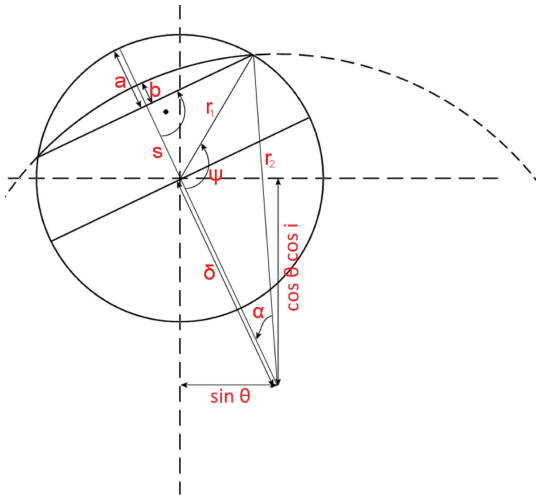

Figure 2. The second type of an occultation when the projected stars' separation is smaller than the radius of the bigger star.

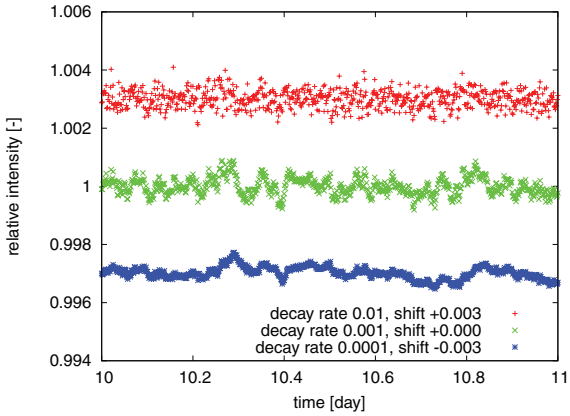

Figure 3. Three examples of the red noise with the same standard deviation and different decay rates $\lambda_{\min}$ of 0.01, 0.001 and 0.0001. Red noise used in our simulations of ground observations is characterized by $\lambda_{\min} = 0.01$.

In general, we add three types of noise to the synthetic light curves. The first one is the photon noise depending on the brightness of an observed eclipsing binary, the second one is the white noise of different origin than the photon noise and the third one is the red noise due to, e.g., the Earth's atmosphere, the instrumentation, etc. The first two are typical for the space-based photometry and all three are expected to be present in the ground-based data.

The red noise is applied using the package for the exact numerical simulation of power-law noises PLNOISE (Milotti 2006, 2007). It is worth noting that the impact of the red noise on the planet discovery space differs with the typical time-scale associated with the red noise. In our code, the red noise is parametrized via the minimal decay rate of the oscillators generating the noise. Even if the standard deviation remains the same, the ET precision changes with the typical time-scale of the red noise. The examples of red noise with different time-scales are shown in Fig. 3.

3 PLANET DISCOVERY SPACE

We simulate a light curve of an eclipsing binary with the photon noise dependent on the brightness of a target and additional Gaussian and red noises if necessary. The level of the latter two is based

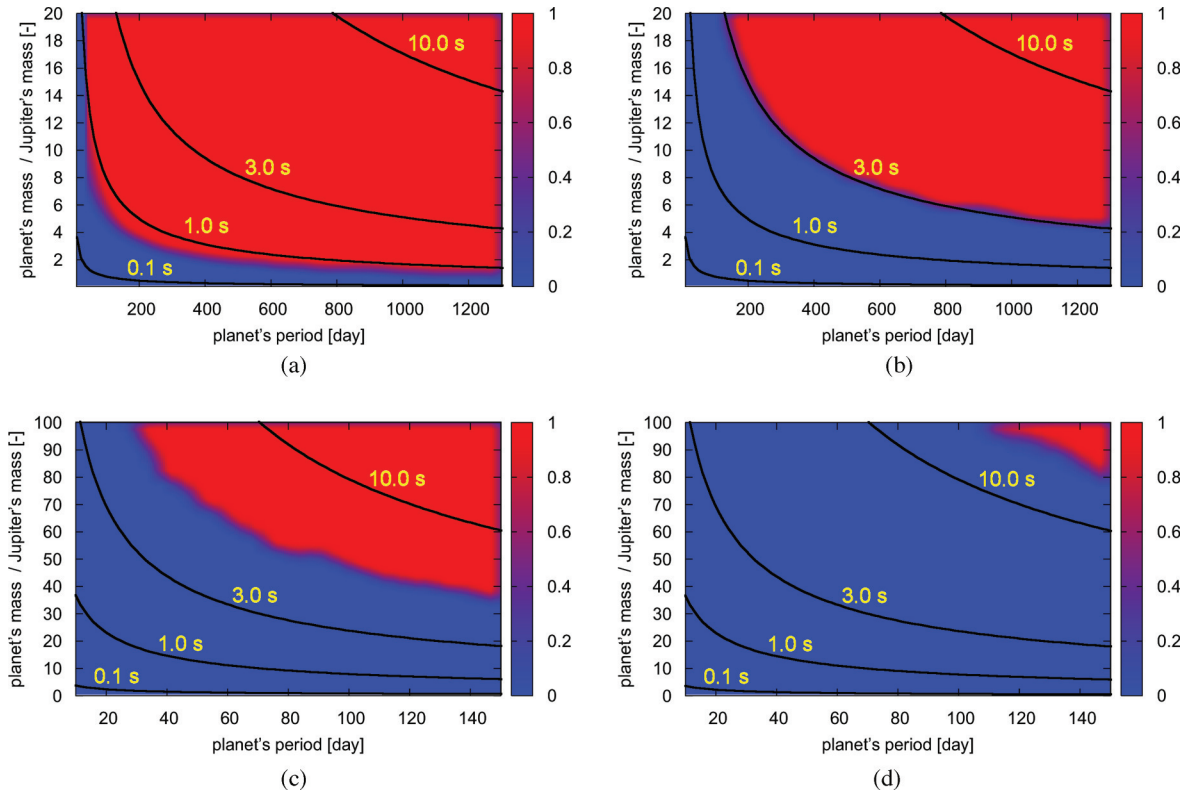

Figure 4. Typical discovery space for *Kepler* (top) and *CoRoT* (bottom). (a) A 9 mag target (the photometric error is $\sigma = 0.035$ mmag) and (b) a 14 mag target ($\sigma = 0.17$ mmag). (c) A 13 mag target ($\sigma = 0.5$ mmag) and (d) a 15 mag target ($\sigma = 1.5$ mmag). One should remember that a measurement is taken every 900 s for *Kepler* which is in the middle of 30 min and 1 min cadences now used and 320 s for *CoRoT*; hence, the total number of measurements varies per one full orbital period of the target binary. Now *Kepler* uses 30 and 1 min cadences but this does not affect the outcome of the simulations. For example, longer integration times provide a smaller photometric error but also a smaller number of measurements per light curve.

on the instrument's characteristic and the place of the observations (space/ground). For such a light curve, a planetary light time disturbance affecting the times of photometric measurements is also added according to the assumed orbital parameters of a circumbinary planet.

The criterion for a detection or a non-detection of a planet is as follows

$$w_j = \frac{1}{\sigma_{x,j}^2}, \quad \overline{x}_w = \frac{\sum_{j=1}^{L} w_j x_j}{\sum_{j=1}^{L} w_j}, \tag{3}$$

$$\sigma_{\rm S} = \sqrt{\frac{\sum_{j=1}^{L} (\overline{x}_w - x_j)^2}{L-1}} \geq 3\max(\sigma_{x,1}, \ldots, \sigma_{x,L}), \tag{4}$$

where x_j is the measured time of the jth eclipse (the t_0 moment of one complete light curve), $\sigma_{x,j}$ denotes its standard deviation and w_j the corresponding weight of such a timing measurement. Finally, $\sigma_{\rm S}$ is calculated to estimate the magnitude of the timing signal which is present in data and this is compared to the largest error of x. Such a procedure allows us to get a quick insight into whether a planetary timing signature may be present in the data set. If inequality (4) is satisfied, it means that a planet is detected and this is denoted with a red colour. A non-detection is denoted with a blue colour. The resulting discovery space is a result of an averaging over a rectangle of 121 neighbouring points. The pure red colour denotes a certain detection (fraction 121/121) and pure blue colour a certain non-detection. Intermediate colours are computed as a linear interpolation between the two basic colours according to a given fraction of detections in a rectangle (see Fig. 4).

Note that such a definition of the detection means that a planetary signal is detected when its timing amplitude A is equal to or larger than $\sim 4\sigma$, where σ is the precision (formal error) of the timing accuracy. Hence, the main factor that defines the discovery space is the precision with which one can measure the moment of one eclipse. Obviously, the longer the data set of timing measurements, the higher is the confidence level with which a planetary signal is detected (for details, see Cumming 2004). For example, since *Kepler* will provide ~ 10 times longer data sets than *CoRoT*, the confidence level of its putative detection would be higher. Or, in other words, for the same confidence level *Kepler* would allow for a detection of smaller amplitudes than *CoRoT*. We have decided to use our simpler, more conservative approach which is not affected by a particular choice of sampling of the timing measurements.

In the above, the time of an eclipse is computed in two ways. The first and classic approach is to use x_j as one of the parameters of a multiparameter least-squares fit of a physical model to the synthetic light curve. In this approach, the parameters of the binary assumed to calculate the light curve are disturbed and used as the starting values of the least-squares parameters. Parameters which are varied and then fitted include the radii r_1, r_2; the inclination i; the orbital reference epoch t_0; the orbital period of the binary P and the luminosity of the secondary $L_{\rm s}$. We use the MINPACK library (Moré, Garbow & Hillstrom 1980; Moré et al. 1984)[1] to carry out a least-squares fitting.

[1]http://www.netlib.org

The simulations can be easily extended to cases with the elliptically distorted stars and include the limb darkening as, for example, in Nelson & Davis (1972). As we have tested, in such a case the results are slightly different after introducing these two effects and the total time required to compute a discovery space is a few times longer. The resulting area of the discovery space corresponding to detectable planets is a bit smaller and moves towards the upper-right corner (see Fig. 4). This is in our opinion the result of the correlations between the increasing number of parameters used in the least-squares fit which often accounts for very subtle effects. For this reason, we believe that it is best to use an approach known from radio pulsar timing and precision radial velocities relying on a reference template pulse or spectrum to measure a timing or radial velocity shift.

In such an approach, the time of an eclipse is computed by comparing a given light curve with a reference light curve obtained by folding all the simulated photometric measurements with the orbital period of a binary. As mentioned, this is an approach used in the radio pulsar timing or in precision radial velocity technique where the cross-correlation function and the reference radio pulse or template spectrum are used to compute a timing shift or a Doppler shift. In our case, in order to compute x_j and its formal error $\sigma_{x,j}$ we use the least-squares formalism. Let us note that for the simpler light-curve model with the spherical binary components and no limb darkening, both approaches result in the same discovery space and for the more complicated binary model case, the approach employing a reference light curve results in a better discovery space (a wider range of detectable planets). Obviously, the second approach will work well only if the light curve is sufficiently stable but then only for such stable light curves/binaries one may hope to detect planets.

The parameters of the binary star, the instruments and the simulated photometric measurements are summarized in Tables 1, 2 and 3, respectively. The discovery space is computed on a dense grid of planetary periods and masses. In Fig. 4, the discovery space is represented by averaging 121 neighbouring points from the grid. The red colour in the diagrams denotes certain detection (fraction 121/121) and the blue one the lack of detection (0/121). All the intermediate colours are computed as a linear interpolation. Black lines in the discovery space show the planet's mass and period which generate a given timing amplitude, A. The equation describing such a line is given by

$$M_{\rm P}(P_{\rm pl}) = \left(\frac{4\pi^2 M_{\rm B}^2}{P_{\rm pl}^2 G}\right)^{\frac{1}{3}} (Ac), \tag{5}$$

where $M_{\rm P}$ and $P_{\rm pl}$ are the mass and period of a planet, respectively, $M_{\rm B}$ is the mass of the binary star, c denotes the speed of light and G is the gravitational constant.

Fig. 4 shows a few examples of a typical discovery space for the *CoRoT* and *Kepler* missions. Each discovery space is a result of one simulation run covering 40 401 points (201 × 201) for which inequality (4) was checked. Based on a discovery space and equation (5), we derive a timing amplitude which fits best to the border between a detection and non-detection. As can be seen in Figs 4(a) and (b), A is an approximation of the actual border and hence the best-fitting value of A is also characterized by its non-zero error σ_A depending on how the real border deviates from A.

Table 1. Binary's star characteristic.

Total luminosity	2 $L_\odot$
Secondary star luminosity	1 $L_\odot$
Total binary star mass	2 $M_\odot$
Effective temperature of binary components	5780 K
Orbital eccentricity	0
Radii	1 $R_\odot$
Orbital period	3 days
Inclination	90 deg
Orbit inclination of a planet	90 deg

Table 2. Instrument characteristic used in our simulations.

Parameter	*CoRoT*	*Kepler*	Ground	Unit
White noise	0.07	0.02	0.35	mmag
Red noise	0	0	0.35	mmag
Band	370–950	430–890	502–587	nm
Integration time	320	900	varies	s
Observing window	150	1461	365	days
Aperture	588	2256	1963.5	cm^2
Throughput	81	81	81	per cent
Target stars (transits)	12–15.5	9–14	–	mag
Target stars (stellar seismology)	6–9	–	–	mag
Target stars (ET)	–	–	6-14	mag

Table 3. Simulation's internal parameters.

Orbital period	From 10 d
Planet mass	From 0.05 $M_{\rm Jupiter}$
Effective no. of simulation points	40 401
No. of light curve active parts	Varies
Red noise dt	1
Red noise nt	0.1
Red noise $\lambda_{\rm min}$	0.01
Red noise $\lambda_{\rm max}$	1

4 *CoRoT* AND *KEPLER*

The ongoing space missions *CoRoT* and *Kepler* aimed to detect transiting planets can in principle be used also to detect circumbinary planets via ET. These missions have the obvious advantage over any ground effort of providing an uninterrupted set of photometric measurements of a time-span of 150 d and 4 yr, respectively. In our simulations, we used the parameters of the missions as described by Costes et al. (2004), Garrido & Deeg (2006) and Auvergne et al. (2009) for *CoRoT* and by Koch et al. (2004) for *Kepler*. They are also summarized in Table 2.

The examples of discovery space for *CoRoT* and *Kepler* are shown in Fig. 4. For other values of L and different photometric errors, see Fig. 5. While both instruments are capable of providing very precise photometry, the resulting discovery space is also affected by the cadence of photometric measurements and the brightness of the targets. Overall, the potential of detecting circumbinary planets with *CoRoT* and *Kepler* comes out somewhat less attractive than one may have hoped for. The simulations allow us to determine the following relations for *CoRoT* and *Kepler*: $A(\sigma) = 10.72\sigma$ $A(\sigma) = 19.14\sigma$, respectively, where σ is the photometric precision of a single measurement in mmag and A the detectable timing amplitude (DTA) in seconds (see Fig. 6).

The potential problem with both missions is the pre-defined target pool. If this is taken into account, despite high photometric precision the chances of detecting a circumbinary, non-transiting planet may be somewhat small. For example, for the *Kepler* mission an

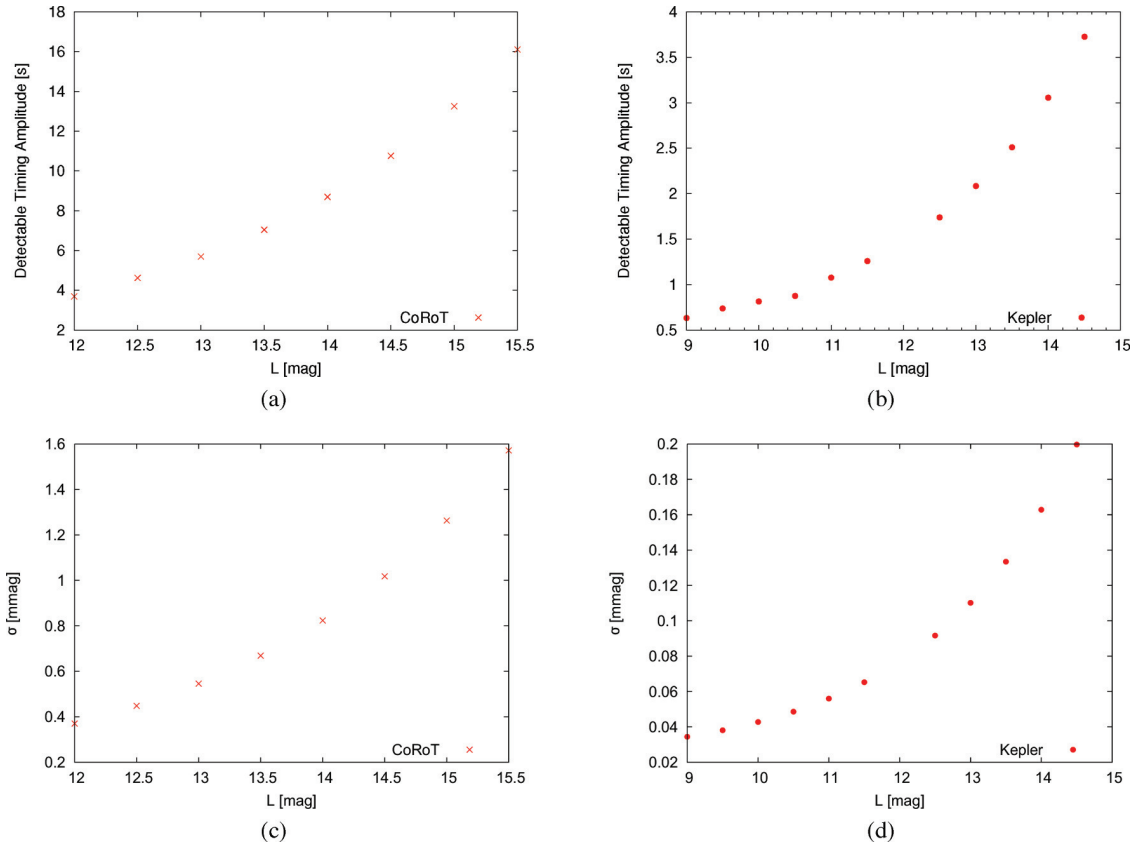

Figure 5. Typical DTA and photometric error for *CoRoT* (a,c) and *Kepler* (b,d) missions and an object with brightness L.

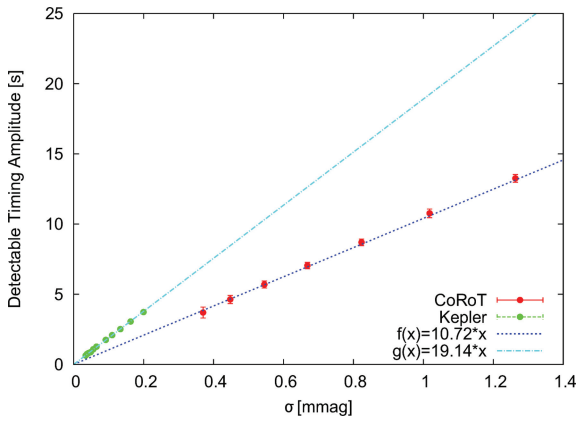

Figure 6. DTA for a given photometric precision for *CoRoT* and *Kepler* missions along with the best-fitting relation. Note that the difference between the two cases is dependent on the cadence of photometric measurements (*CoRoT* ∼ 320 and *Kepler* ∼ 900 s).

upper limit to detectable circumbinary planets may be estimated as follows:

$$n_{\rm P} = n_* p_* p_J = 10^5 \times 0.00016 \times 0.06 = 0.96, \quad (6)$$

where n_* is the number of targets, $n_* \approx 10^5$,[2] p_* is the ratio of eclipsing detached binary stars to all stars, $p_* \approx 0.00016$ (Paczyński et al. 2006), and p_J is the percentage of stars having giant planets (assuming that it is the same as for single stars), $p_J \approx 0.06$; equation (6) does not take into account the probability of detecting a planet with a given mass and period via ET. Clearly, in order to detect circumbinary planets using ET one may have to turn to the ground-based observations where the target pool can be carefully selected and fine-tuned to provide for the highest possible chances of detecting circumbinary planets. However, let us note that in the above we used a percentage of *detached* binaries in the All-Sky Automated Survey (ASAS) catalogue. If one is willing to try the presumably less stable contact binaries as well, then p_* increases to ∼0.00065 according to the results from the ASAS sample (Paczyński et al. 2006). Even more optimistic preliminary results come from the *Kepler* and *CoRoT* fields for which the percentage of eclipsing binaries is ∼0.007 (Deeg & Doyle, private communication). In such a case, the number of potentially detectable planets would rise to ∼40.

[2]http://kepler.nasa.gov/

5 OBSERVATIONS FROM THE GROUND

Performing numerical simulations that would aim to answer all or almost all questions related to a search for circumbinary planets using ground-based ET is not practical. Possible observing scenarios are highly dependent on the choice of a target, its parameters and the coordinates of an observatory. Such simulations can be carried out if the target pool and the observatory are already chosen. For these reasons, we present below a few typical problems one may encounter when performing a ground-based ET survey and analyse them through numerical simulations. These results are an essence of a much larger set of simulations we carried out.

The two main differences between the space- and ground-based surveys are the presence of red noise due to predominately the

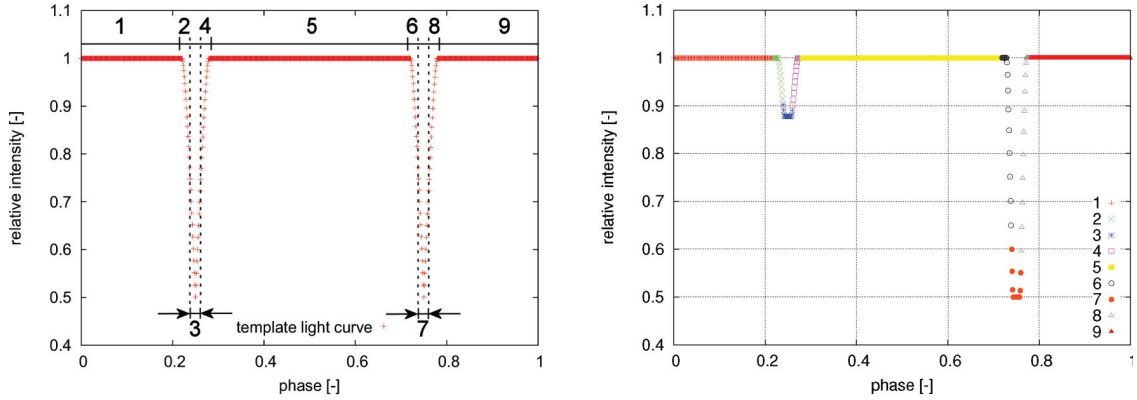

Figure 7. Light-curve templates for simulations exploring an influence of the different parts of light curves on DTA. Figure (a) The template of V-shape eclipses and (b) flat bottom eclipses.

atmosphere and the typically very incomplete light curves one obtains with a ground-based telescope for a detached eclipsing binary that typically has an orbital period much longer than the duration of a night. For our reference binary (Table 1), we simulated two types of light curves: one with V-shaped eclipses (the parameters exactly as in Table 1) and one with eclipses with flat bottoms. In the latter case, we assumed a radius ratio of 0.5 while keeping $L_2 = 0.5$. To the simulated photometric measurements we added red noise with an rms of 0.35 mmag, white noise with an rms of 0.35 mmag and photon noise depending on the actual momentary brightness. We divided the light curves into nine parts to explore which parts when present have the largest impact on the DTA (see Figs 7a and b). In the simulations, we removed parts of the light curves and used such incomplete light curves to measure the times of eclipse. All the permutations possible without repetition were used for sets ranging from one to nine light curve elements. Afterwards, an average DTA was calculated. Whenever a DTA could not be computed, the result was set to 20 s by default. The results are shown in Tables 4 and 5. In the tables, the columns correspond to the parts of the light curve which were present and the rows correspond to the total number of parts present ('active') in a light curve. This approach allows us to easily determine the most valuable parts of a light curve and establish which sets of them when present provide even better results.

In the case of V-shaped eclipses, the most important are parts 3 and 7 in Fig. 7(a) which correspond to the middle parts of eclipses. Next come ingress and egress. For the eclipses with flat bottoms, the most valuable parts are 6 and 8 in Fig. 7(a) (ingress and egress of the deeper eclipse). Altogether, most of the timing information can be derived by just observing the entire eclipses. This is consistent

Table 4. Impact of different parts of a light curve and their combinations on DTA (in seconds) for a V-shaped eclipse shown in Fig. 7(a). DTA of 20 s means that a timing measurement was not possible.

No. of active parts/part no.	1	2	3	4	5	6	7	8	9
1	20.00	6.28	3.74	8.08	20.00	8.16	4.88	8.36	20.00
2	9.95	5.27	3.53	6.34	9.96	6.25	4.26	6.54	9.97
3	6.02	4.50	3.32	5.03	6.01	4.99	3.81	5.13	6.03
4	4.46	3.91	3.12	4.16	4.45	4.15	3.47	4.20	4.47
5	3.71	3.47	2.96	3.59	3.71	3.56	3.20	3.59	3.71
6	3.47	3.36	3.10	3.50	3.58	3.50	3.31	3.52	3.59
7	2.92	2.87	2.70	2.90	2.92	2.89	2.80	2.90	2.93
8	2.67	2.65	2.58	2.66	2.67	2.66	2.62	2.66	2.67
9	2.52	2.52	2.52	2.52	2.52	2.52	2.52	2.52	2.52

Table 5. Impact of different parts of a light curve and their combinations on DTA (in seconds) for an eclipse with a flat bottom shown in Fig. 7(b). DTA of 20 s means that a timing measurement was not possible.

No. of active parts/part no.	1	2	3	4	5	6	7	8	9
1	20.00	6.88	20.00	20.00	20.00	4.29	9.60	4.21	20.00
2	12.89	6.76	11.33	11.46	14.51	3.80	8.10	3.87	12.89
3	8.52	6.75	7.61	7.58	9.52	3.52	5.43	3.65	8.51
4	5.14	4.87	5.14	4.85	5.15	3.29	4.51	3.39	5.17
5	4.77	4.49	4.56	4.53	4.72	3.16	3.91	3.22	4.72
6	3.54	3.48	3.51	3.52	3.54	2.93	3.36	3.00	3.53
7	3.06	3.04	3.05	3.06	3.06	2.78	3.00	2.82	3.06
8	2.76	2.75	2.75	2.75	2.75	2.65	2.74	2.66	2.76
9	2.55	2.55	2.55	2.55	2.55	2.55	2.55	2.55	2.55

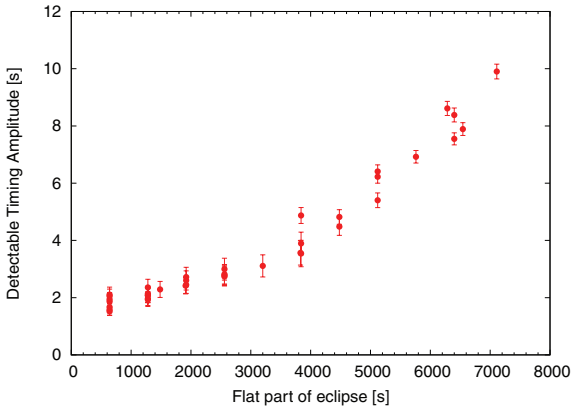

Figure 8. Duration of the flat part of an eclipse and DTA.

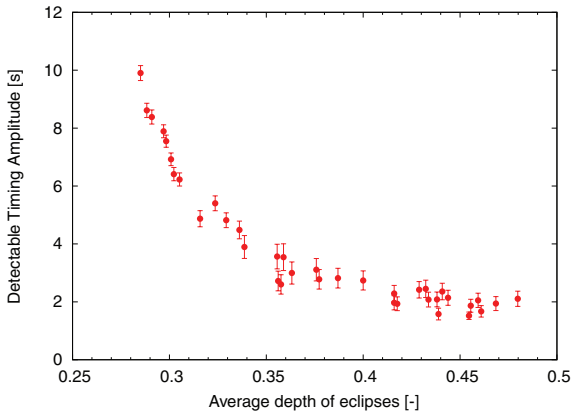

Figure 9. Depth of an eclipse and DTA.

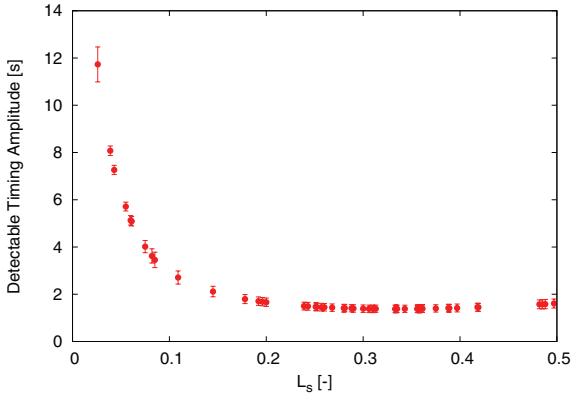

Figure 10. Impact of the second star's luminosity L_S in units of the primary star's luminosity on the DTA.

with common sense and is easily achievable from the ground. Let us also note that in the simulations we used the first type of red noise from Fig. 3. We also determined that its impact on the DTA is comparable to white noise with an rms twice as large (i.e. 0.7 mmag).

In another set of simulations, we tested a number of features of an eclipse that affect the timing precision and detectable amplitude. We tested the impact of the duration of a flat part of an eclipse (Fig. 8), the impact of the eclipse's depth (Fig. 9), the impact of the duration of a V-shaped eclipse, the impact of the secondary star's luminosity (Fig. 10) and the radius ratio (Fig. 11) on the DTA. The conclusion is that it is preferable to observe V-shaped short-lasting

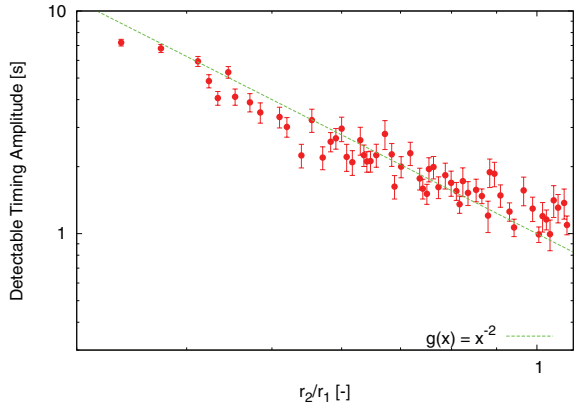

Figure 11. Detectable timing amplitude as a function of the ratio of radii of the secondary to primary star (r_2/r_1). In these simulations, the parameters for the ground-based case were used.

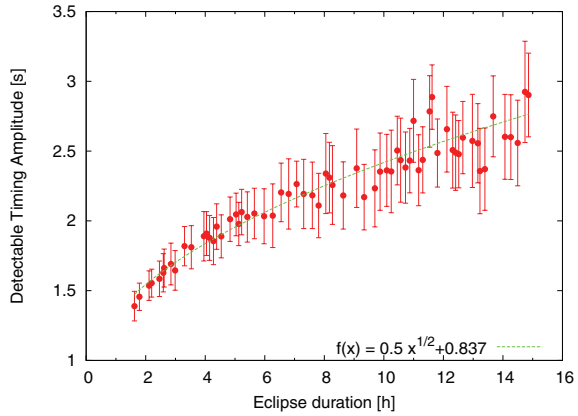

Figure 12. Duration of an eclipse and DTA. The solid line represents the analytic approximation by Doyle & Deeg (2004).

and deep eclipses to maximize DTA which is not an unexpected result.

Let us note that Doyle & Deeg (2004) derived an equation allowing one to estimate an ET precision assuming that the eclipse has a simple triangular shape:

$$\delta_{t_0} \approx \delta_L \frac{T_{\rm ec}}{2\Delta L\sqrt{N}}, \tag{7}$$

where $T_{\rm ec}$ is the duration of an eclipse, N is the number of photometric measurements taken during $T_{\rm ec}$ and ΔL is the relative depth of the eclipse. Our simulations prove that this is a good approximation. This can be seen in Fig. 12 where one should note that after introducing the integration time $T_{\rm int}$, we have $N = T_{\rm ec}/T_{\rm int}$ and equation (7) can be rewritten as

$$\delta_{t_0} \approx \delta_L \frac{\sqrt{T_{\rm ec}T_{\rm int}}}{2\Delta L}. \tag{8}$$

In the above, $T_{\rm int}$ is constant, the DTA is approximately equal to δ_{t_0} and the square-root relation between δ_{t_0} and $T_{\rm ec}$ is visible.

We conclude the simulations with two representative figures for a ground-based survey based on a 0.5-m telescope. Fig. 13 shows DTA and Fig. 14 a typical photometric error due to the photon noise for our test scenario.

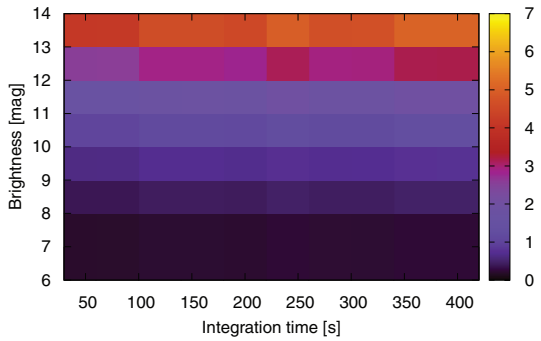

Figure 13. DTA as a function of the integration time and brightness of the target for a ground-based effort.

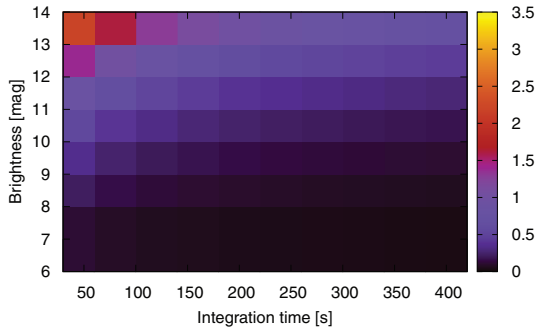

Figure 14. Photometric precision in mmag as a function of the integration time and brightness of the target for a ground-based effort.

6 CONCLUSIONS

In order to detect giant circumbinary planets around eclipsing stars, a timing precision of the order of 0.1–1 s is necessary. The *Kepler* and *CoRoT* missions are capable of providing photometric precision sufficient to reach such a timing precision. However, in both cases what makes the detections challenging is a pre-defined target pool. In the case of *CoRoT*, typical targets are quite faint and the duration of an observing window is only 150 d which effectively limits the detection capabilities to brown dwarfs. In the case of *Kepler*, the target pool puts an upper limit of potentially detectable circumbinary gas giants at about 40 in the best-case scenario. This number does not take into account the orbital and physical parameters of circumbinary planets (such as masses). Hence, the more realistic upper limit is expected to be several times lower. Nevertheless, both missions may still deliver us a detection of a circumbinary planet via ET. It seems that the best strategy to detect circumbinary planets around eclipsing binary stars is by carrying out a ground-based survey for which targets can be carefully pre-selected. Such a survey would have to employ several 0.5-m class telescopes to be efficient. As the survey would typically focus on the shorter period detached eclipsing binary stars (see Fig. 12), it would target a different set of targets than a radial-velocity-based survey.

In Fig. 15, we compare planet detection capabilities of the radial velocity, astrometry and ET. ET which is essentially a one-dimensional astrometric measurement is complementary to the radial velocity technique and as we have demonstrated one is able to achieve a timing precision sufficient to detect giant planets. Finally, let us note that two circumbinary planets around an eclipsing binary HW Vir (Lee et al. 2009), a circumbinary brown dwarf around an eclipsing binary HS 0705+6700 (Qian et al. 2009) and a giant planet around an eclipsing polar DP Leo (Qian et al. 2010) were

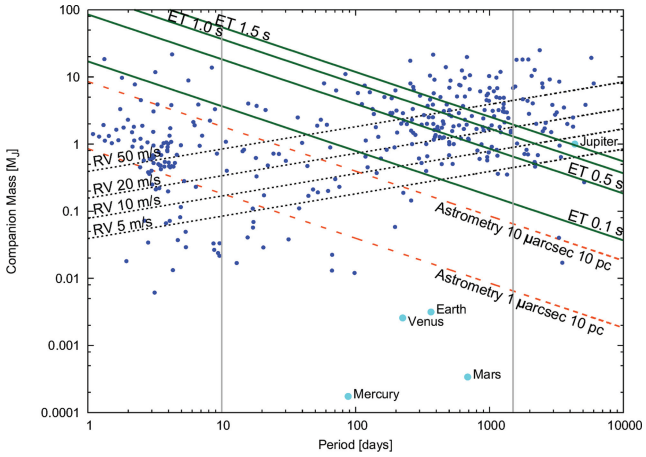

Figure 15. Discovery space for circumbinary planets around a binary star composed of two Sun-like stars. Known exoplanets are marked with dots. The two vertical lines correspond to the shortest stable orbit for this case (Dvorak, Froeschle & Froeschle 1989; Holman & Wiegert 1999) and 4 yr.

claimed to be detected by means of ET. However, it is hard to judge if these cases of timing variation are really caused by substellar companions and not by an unknown quasi-periodic phenomenon. Nevertheless, this is yet another proof that ET is becoming a useful tool for detecting subtle timing variations.

ACKNOWLEDGMENTS

This work is supported by the Foundation for Polish Science through a FOCUS grant, by the Polish Ministry of Science and Higher Education through grant no. N203 005 32/0449 and by the European Social Fund and the national budget of the Republic of Poland within the framework of the Integrated Regional Operational Programme, Measure 2.6. Regional innovation strategies and transfer of knowledge – an individual project of the Kuyavian-Pomeranian Voivodship 'Scholarships for Ph.D. students 2008/2009 – IROP'

REFERENCES

Alonso R. et al., 2008, A&A, 482, L21
Auvergne M. et al., 2009, A&A, 506, 411
Costes V., Bodin P., Levacher P., Auvergne M., 2004, in Warmbein B., ed., 5th International Conference on Space Optics. ESA Publications, Noordwijk, p. 281
Cumming A., 2004, MNRAS, 354, 1165
Deeg H. J., Ocaña B., Kozhevnikov V. P., Charbonneau D., O'Donovan F. T., Doyle L. R., 2008, A&A, 480, 563
Doyle L. R., Deeg H. J., 2004, in Norris R., Stootman F., eds, Proc. IAU Symp. 213, Bioastronomy 2002: Life Among the Stars. Kluwer, Dordrecht, p. 80
Dvorak R., 1984, Celest. Mech., 34, 369
Dvorak R., Froeschle C., Froeschle C., 1989, A&A, 226, 335
Garrido R., Deeg H. J., 2006, Lecture Notes Essays Astrophys., 2, 27
Holman M. J., Wiegert P. A., 1999, AJ, 117, 621
Koch D. G. et al., 2004, Proc. SPIE, 5487, 1491
Lee J. W., Kim S.-L., Kim C.-H., Koch R. H., Lee C.-U., Kim H. I., Park J.-H., 2009, AJ, 137, 3181
Milotti E., 2006, Comput. Phys. Communications, 175, 212
Milotti E., 2007, Phys. Rev, 75, 011120
Moré J. J., Garbow B. S., Hillstrom K. E., 1980, User Guide for MINPACK-1, Argonne National Laboratory Report ANL-80-74

Moré J. J., Sorensen D. C., Hillstrom K. E., Garbow B. S., 1984, in Cowell W. J., ed., The MINPACK Project, in Sources and Development of Mathematical Software. Prentice-Hall, p. 88
Muterspaugh M. W., Konacki M., Lane B. F., Pfahl E., 2007, preprint (astro-ph/0705.3072)
Nelson B., Davis W. D., 1972, ApJ, 174, 617
Paczyński B., Szczygieł D. M., Pilecki B., Pojmański G., 2006, MNRAS, 368, 1311
Qian S.-B., Dai Z.-B., Liao W.-P., Zhu L.-Y., Liu L., Zhao E. G., 2009, ApJ, 706, L96
Qian S.-B., Liao W.-P., Zhu L.-Y., Dai Z.-B., 2010, ApJ, 708, L66

This paper has been typeset from a TEX/LATEX file prepared by the author.